



# A Study of Magnetized White Dwarf + Helium Star Binary Evolution to Type Ia Supernovae

Zhe Cui<sup>1</sup>  and Xiang-Dong Li<sup>1,2</sup>

<sup>1</sup> School of Astronomy and Space Science, Nanjing University, Nanjing 210023, China

<sup>2</sup> Key Laboratory of Modern Astronomy and Astrophysics, Nanjing University, Ministry of Education, Nanjing 210023, China; [lixd@nju.edu.cn](mailto:lixd@nju.edu.cn)

Received 2021 October 6; revised 2021 November 1; accepted 2021 November 4; published 2022 February 2

## Abstract

The white dwarf (WD) + helium (He) star binary channel plays an important role in the single degenerate scenario for the progenitors of type Ia supernovae (SNe Ia). Previous studies on the WD + main sequence star evolution have shown that the magnetic fields of WDs may significantly influence their accretion and nuclear burning processes. In this work we focus on the evolution of magnetized WD + He star binaries with detailed stellar evolution and binary population synthesis (BPS) calculations. In the case of magnetized WDs, the magnetic fields may disrupt the inner regions of the accretion disk, funnel the accretion flow onto the polar caps and even confine helium burning within the caps. We find that, for WDs with sufficiently strong magnetic fields, the parameter space of the potential SN Ia progenitor systems shrinks toward shorter orbital periods and lower donor masses compared with that in the non-magnetized WD case. The reason is that the magnetic confinement usually works with relatively high mass transfer rates, which can trigger strong wind mass loss from the WD, thus limiting the He-rich mass accumulation efficiency. The surviving companion stars are likely of low-mass at the moment of the SN explosions, which can be regarded as a possible explanation for the non-detection of surviving companions after the SNe or inside the SN remnants. However, the corresponding birthrate of Galactic SNe Ia in our high-magnetic models is estimated to be  $\sim(0.08\text{--}0.13) \times 10^{-3} \text{ yr}^{-1}$  ( $\sim 0.17\text{--}0.28 \times 10^{-3} \text{ yr}^{-1}$  for the non-magnetic models), significantly lower than the observed Galactic SN Ia birthrate.

*Key words:* stars: evolution – (stars:) supernovae: general – (stars:) binaries: general – stars: magnetic field – (stars:) white dwarfs

## 1. Introduction

Type Ia supernovae (SNe Ia) are among the most violent events in the universe, which present us the possibilities to probe the evolutionary history of cosmic expansion over the past ten billion years (Riess et al. 1998; Perlmutter et al. 1999). They are regarded as the standard candles for cosmological measurements benefiting from their unified light curves, to derive the values of cosmological parameters (such as the mass density  $\Omega_M$ , the dark energy density  $\Omega_\Lambda$  and the Hubble constant  $H_0$ ) (Branch & Tammann 1992; Hamuy et al. 1993; Hamuy et al. 1996; Nomoto et al. 1997), setting off an upsurge in the study of dark energy (Alam et al. 2007; Riess et al. 2007; Rest et al. 2014; Demianski et al. 2019).

Spectroscopic and photometric studies prefer SNe Ia to be the runaway thermonuclear fusion of carbon and oxygen in white dwarfs (WDs) once their masses reach the Chandrasekhar mass ( $M_{\text{ch}}$ ) limit (Hoefflich & Khokhlov 1996; Nugent et al. 1997). However, the nature of their progenitors is still under debate, and the proposed progenitor scenarios can only explain part of the observations, such as the properties of the host galaxies, the delay times, the birthrates, the surviving companion stars, etc. (Cappellaro et al. 1997;

Iwamoto et al. 1999; Mannucci et al. 2005; Mazzali et al. 2007; Maoz et al. 2011; Wang & Han 2012; Ruiz-Lapuente 2014; Maeda & Terada 2016; Soker & Gilkis 2017; Patat & Hallakoun 2018). Several progenitor scenarios are currently under discussion, but are all confronted with an increasing number of challenges (Maoz & Mannucci 2012).

In the so-called double degenerate (DD) scenario, two CO WDs undergo a dynamical coalescence (Iben & Tutukov 1984) owing to orbital shrinkage caused by gravitational wave radiation, resulting in a combined mass exceeding  $M_{\text{ch}}$  and a subsequent SN Ia. This scenario is supported by some observational facts such as the absence of H emission lines in the early- and nebular-phase spectra of SNe Ia (Leonard 2007; Brown et al. 2012; Shappee et al. 2013; Lundqvist et al. 2015; Olling et al. 2015; Sand et al. 2018; Dimitriadis et al. 2019; Tucker et al. 2019), and the non-detection of a surviving companion star in the relatively close supernova remnants (SNRs) (Schaefer & Pagnotta 2012; Kerzendorf et al. 2013; Kerzendorf et al. 2018; Ruiz-Lapuente et al. 2018). The predicted occurrence rates and delay time distribution (DTD) of SNe Ia from the DD scenario are consistent with observations in both young and old stellar populations (Ruiter et al. 2009;

Maoz et al. 2010; Liu et al. 2016; Liu et al. 2018; Yungelson & Kuranov 2017). However, the coalescence of double WDs may also trigger an off-center convective carbon-burning, yielding a high-mass O/Ne WD or collapse to a neutron star, rather than an SN Ia (Nomoto & Iben 1985; Shen et al. 2012).

Alternatively, the single degenerate (SD) scenario (Whelan et al. 1973) assumes that a CO WD accumulates hydrogen- and/or helium-rich material on its surface by rapidly accreting from its non-degenerate companion, which is either a main-sequence (MS) star, a sub-giant star, a red giant (RG) star or a He star. Under specific conditions, the accreted material can burn steadily on the surface of the WD, which will eventually explode as an SN Ia when its mass reaches  $M_{\text{ch}}$  (Nomoto 1982; Hachisu et al. 1996; Li & van den Heuvel 1997; Han & Podsiadlowski 2004; Lü et al. 2009; Wang & Han 2012). This scenario is capable of explaining the observational homogeneity of SNe Ia (Hamuy et al. 1991), since the SNe Ia realized through this channel are the thermonuclear explosions of similar-mass CO WDs. However, the diversities in the maximum luminosities, light-curve shapes and the spectra of SNe Ia would imply other evolutionary channels (Phillips 1993; Branch et al. 1996; Hamuy et al. 1996; Umeda et al. 1999). For the SD scenario, the mass transfer through Roche-lobe overflow (RLOF) is crucial since the WD can accumulate mass only when the accretion rate  $\dot{M}_{\text{acc}}$  is within a narrow range for steady hydrogen and helium burning (e.g., Nomoto 1982; Kato & Hachisu 2004; Brooks et al. 2016). The predicted SN Ia birthrates (a few  $\times 10^{-4} \text{ yr}^{-1}$ ) (Ruiter et al. 2009; Wang et al. 2017) are an order of magnitude lower than the observed ones (a few  $\times 10^{-3} \text{ yr}^{-1}$ ) (Cappellaro & Turatto 1997; Patat & Hallakoun 2018). Moreover, the observations of nearby SNe Ia and SNRs provide an upper limit on the luminosity of the surviving companion star, setting stringent constraints on the parameter space of the progenitor binaries (Badenes et al. 2007; Maoz & Mannucci 2008; Kerzendorf et al. 2009; Li et al. 2011; Kelly et al. 2014; Maoz et al. 2014; Ruiz-Lapuente 2014).

Magnetism accounts for a non-negligible incidence in observed WDs. With the advent of the Sloan Digital Sky Survey and other large-scale spectroscopic surveys, the numbers of known single and binary magnetic WDs (MWDs) with magnetic fields  $B$  in the range  $\sim 10^6$ – $10^9$  G have increased to more than 600 and 200, respectively (Wickramasinghe & Ferrario 2000; York et al. 2000; Gänsicke et al. 2002; Schmidt et al. 2003; Vanlandingham et al. 2005; Külebi et al. 2009; Sion et al. 2014; Kepler et al. 2015; Ferrario et al. 2015; Ferrario et al. 2020). Magnetic cataclysmic variables (MCVs) make up about 25% of the known CVs in the magnitude-limited samples and even as high as 36% within 150 pc (Ferrario et al. 2015; Pala et al. 2020). Observations and studies of MCVs and super-soft X-ray sources (SSSs) have revealed the influence of magnetic

field on the WD binary evolution (Osborne et al. 2001; Ferrario et al. 2015). For instance, MCVs generally behave as much stronger X-ray emitters than non-magnetic ones. The magnetic fields of WDs have also been taken into account in the study of the SN Ia formation mechanisms. Neunteufel et al. (2017) indicate that helium ignition in (rotating) weakly magnetized CO WDs may lead to fast and faint hydrogen-free SN explosions. Moreover, since the accreted material is funneled onto a small portion of the WD surface by the magnetic field lines, thermonuclear burning on magnetic WDs could be different from that on non-magnetic WDs even at the same accretion rate. For example, a relatively low accretion rate of  $\sim 10^{-9} M_{\odot} \text{ yr}^{-1}$  may be high enough to sustain local stable hydrogen burning on MWDs (Schaefer & Collazzi 2010), implying that magnetism may significantly influence the evolution of accreting WDs (also see discussion in Wheeler (2012) and Ablimit et al. (2014)). Ablimit & Maeda (2019a, 2019b) investigated the MWD + MS star binary evolution to SNe Ia and showed that, with the magnetic field confinement, the initial parameter spaces of the SN Ia progenitor systems become larger and the surviving companion stars could be dimmer and lighter compared with those in the non-magnetic models, and these features are compatible with non-detection of surviving companion stars in nearby SNe and SNRs as mentioned above. Accretion of He-rich matter onto a WD from its H-depleted donor is related to some interesting events. For example, the He nova V445 Puppis and the X-ray pulsating companion of HD 49798 are both suggested to be candidates for SN Ia progenitors (Kato et al. 2008; Wang & Han 2010). In addition, hyper-velocity stars such as US 708 (HVS2) (Hirsch et al. 2005) may be the surviving donors of SNe Ia from the WD + He star channel (Wang & Han 2009). As the WD + He star channel also plays an important role in the SD scenario (Wang et al. 2010), it is interesting to examine the influence of magnetism on the evolution of He-accreting MWDs, and this is the objective of our work.

The rest of this paper is organized as follows. We present our methods of simulating the evolution of WD + He binary systems in Section 2, together with some representative examples of MWD + He binary evolution under different magnetic field strengths of the WDs. Section 3 demonstrates the calculated results with a binary population synthesis (BPS) method on the distribution of the progenitor systems and the surviving companions. We summarize our results and conclude in Section 4.

## 2. The Evolution of WD + He Binary Systems

### 2.1. Non-magnetic WDs

In the case of non-magnetic WDs, we simulate the WD + He binary evolution under the optically thick wind model (Hachisu et al. 1996), similar to Wang et al. (2009). The mass growth

rate  $\dot{M}_{\text{wd}}$  of the accreting WDs can be expressed as  $\dot{M}_{\text{wd}} = \eta_{\text{He}} \dot{M}_{\text{acc}} = \eta_{\text{He}} |\dot{M}|$ , where  $\eta_{\text{He}}$  and  $\dot{M}$  are the He-rich mass accumulation efficiency and the mass transfer rate, respectively. We use the results of Kato & Hachisu (2004) for the  $\eta_{\text{He}}$  during He-shell flashes, summarized as follows.

(1) If  $|\dot{M}|$  exceeds the critical value  $\dot{M}_{\text{crit}} = 7.2 \times 10^{-6} (M_{\text{wd}}/M_{\odot} - 0.6) M_{\odot} \text{yr}^{-1}$  (Nomoto 1982),  $\dot{M}_{\text{wd}}$  is limited to  $\dot{M}_{\text{crit}}$ , and the rest of the transferred matter is blown away from the system in the form of isotropic winds at a rate of  $\dot{M}_{\text{wind}} = |\dot{M}| - \dot{M}_{\text{crit}}$ , taking the specific angular momentum of the WD. Then  $\eta_{\text{He}} = \dot{M}_{\text{crit}}/|\dot{M}|$ .

(2) If  $|\dot{M}|$  drops below the minimum accretion rate of weak helium flashes  $\dot{M}_{\text{low}}$  (Woosley et al. 1986), the thermal timescale of the cool and dense WD shell is longer than the accretion-heating timescale, thus the helium shell flashes will be too strong to leave any combustion products. In this situation  $\eta_{\text{He}} = 0$ .

(3) If  $\dot{M}_{\text{stable}} < |\dot{M}| < \dot{M}_{\text{crit}}$ , the accreted helium can burn steadily at a rate of  $|\dot{M}|$ , thus  $\eta_{\text{He}} = 1$ ; if  $\dot{M}_{\text{low}} < |\dot{M}| < \dot{M}_{\text{stable}}$ , weak helium flashes will take place with  $0 < \eta_{\text{He}} < 1$ , which is  $|\dot{M}|$  and  $M_{\text{wd}}$  dependent. In this case, we use the fitted formulae for  $\eta_{\text{He}}$  in Kato & Hachisu (2004). Since the maximum accretion rate calculated in Kato & Hachisu (2004) is  $10^{-5.8} M_{\odot} \text{yr}^{-1}$ , we simply assume  $\eta_{\text{He}} = 1$  when  $10^{-5.8} M_{\odot} \text{yr}^{-1} < |\dot{M}| < \dot{M}_{\text{crit}}$ .

Several groups have performed numerical simulations of He shell burning processes on WDs, and we note that there is no consensus on the He-rich mass accumulation efficiency in the literature. Taking into account the thermal response of He-accreting WDs, Piersanti et al. (2013), Piersanti et al. (2014) made long-term evolutionary calculations for WDs with initial masses of  $0.6\text{--}1.1 M_{\odot}$ , and obtained  $\eta_{\text{He}}$  during different accretion regimes. By introducing the super-Eddington wind loss, Wang et al. (2015) calculated the values of  $\eta_{\text{He}}$  with the WD masses ranging from 0.6 to  $1.35 M_{\odot}$ . The critical accretion rate for stable He-shell burning in Wang et al. (2015) is substantially lower than that in Piersanti et al. (2013), Piersanti et al. (2014). For example, for a  $1.2 M_{\odot}$  WD accreting at a rate of  $\sim 3.9 \times 10^{-6} M_{\odot} \text{yr}^{-1}$ , the He-shell can burn steadily according to Piersanti et al. (2013, 2014), while according to Wang et al. (2015) there will be strong super-Eddington winds from the WD. In their evolutionary calculations, Brooks et al. (2016) resolved the full stellar structures of both binary components, and employed the optically thick wind scenario in the wake of the WD's inflating instead of using a form of  $\dot{M}_{\text{crit}}$  as prescribed by Nomoto (1982). Their calculated values of  $\eta_{\text{He}}$  are generally between those of Kato & Hachisu (2004) and Wang et al. (2015). Assuming that there are super-Eddington winds during multi-cycle He-shell flashes, Wu et al. (2017) also calculated the values of  $\eta_{\text{He}}$ , and found them to be lower than those in Kato & Hachisu (2004).

Considering the uncertainties in  $\eta_{\text{He}}$  and in order to explore how  $\eta_{\text{He}}$  influences the evolution of the WD + He binaries, we

also make evolutionary calculations by adopting the prescription of Wang et al. (2015). In Wang et al. (2015) the optically thick wind in Kato & Hachisu (2004) is replaced by the super-Eddington wind, which can significantly reduce  $\eta_{\text{He}}$ , so they can be regarded as representing the high and low ends of the actual values of  $\eta_{\text{He}}$ . In the following we call them the WL and KH prescriptions, respectively.

## 2.2. Magnetic WDs

For non-magnetic WDs, we assume that the accretion disk extends to the surface of WDs and then the accreted matter is spherically symmetrically distributed on the WDs; but for MWDs with magnetic fields of  $B \sim 10^6$  G (for intermediate polars) or  $\geq 10^7$  G (for polars), the strong magnetic fields can disrupt part or all of the accretion disk and force the material to fall onto the poles of the WDs. This can be described as polar cap accretion (Hameury et al. 1986).

For accreting MWDs with dipolar magnetic fields, the magnetic pressure is expressed as (Frank et al. 2002)

$$P_{\text{mag}} = \frac{(BR_{\text{wd}}^3)^2}{8\pi r^6}, \quad (1)$$

where  $r$  is the radial distance from the center of the MWD, and  $R_{\text{wd}}$  is the radius of the MWD. Equation (1) indicates that  $P_{\text{mag}}$  increases rapidly as the accreted material approaches the WD's surface. At the magnetospheric radius  $R_M$ ,  $P_{\text{mag}}$  exceeds the ram pressure of the accreting matter, and the motion of the accreted matter starts to be controlled by the magnetic fields. Hence the magnetic confinement condition can be expressed as

$$\frac{(BR_{\text{wd}}^3)^2}{8\pi R_M^6} \geq \frac{(2GM_{\text{wd}})^{1/2} \dot{M}}{4\pi R_M^{5/2}} \quad (2)$$

or rewritten as

$$B \geq B_{\text{cap}} \simeq 9.8 \times 10^3 \left( \frac{\dot{M}}{10^{-10} M_{\odot} \text{yr}^{-1}} \right)^{1/2} \times \left( \frac{M_{\text{wd}}}{M_{\odot}} \right)^{1/4} \left( \frac{R_{\text{wd}}}{5 \times 10^8 \text{cm}} \right)^{-5/4} \text{G}, \quad (3)$$

where the term on the right-hand-side of Equation (2) is the ram pressure,  $G$  is the gravitational constant and the value of  $R_{\text{wd}}$  can be calculated from the mass–radius relation of WDs (Livio 1983).

To confine the accreted material within the polar caps without spreading over the MWD surface, the magnetic pressure should be larger than the pressure  $P_b$  at the base of the accreted matter, under which the accreted material can be ignited, so the magnitude of  $B$  should satisfy the following

requirement

$$\begin{aligned}
 B \geq B_{\text{conf}} &\simeq 9.3 \times 10^7 \left( \frac{R_{\text{wd}}}{5 \times 10^8 \text{ cm}} \right) \\
 &\times \left( \frac{P_{\text{b}}}{5 \times 10^{19} \text{ dyn cm}^{-2}} \right)^{7/10} \left( \frac{M_{\text{wd}}}{M_{\odot}} \right)^{-1/2} \\
 &\times \left( \frac{\dot{M}}{10^{-10} M_{\odot} \text{ yr}^{-1}} \right)^{-1/2} \text{ G}. \quad (4)
 \end{aligned}$$

For He-shell burning  $P_{\text{b}} = \frac{GM_{\text{wd}}M_{\text{ign}}}{4\pi R_{\text{wd}}^4}$ , where  $M_{\text{ign}}$  is the minimum He-shell mass for hydrodynamic He-shell burning. We calculate the values of  $P_{\text{b}}$  as a function of  $M_{\text{wd}}$  from the numerical simulations of He-shell burning by Shen & Bildsten (2009).

In polar coordinates  $(r, \theta)$  with the origin located at the WD's center, the dipolar magnetic field lines follow the geometry  $r = C \sin^2 \theta$ , where  $C$  is a constant labeling all the field lines emanating from a particular latitude on the WD. The area of the polar cap is estimated to be  $\simeq \pi R_{\text{wd}}^2 \sin^2 \beta$ , where  $\beta$  is the half-angle of the polar cap. The fraction  $f_{\text{pc}}$  of the area of the two polar caps in the total WD surface area can be expressed to be (Frank et al. 2002)

$$f_{\text{pc}} \simeq \frac{2 \cdot \pi R_{\text{wd}}^2 \sin^2 \beta}{4\pi R_{\text{wd}}^2} \simeq \frac{R_{\text{wd}} \cos^2 \gamma}{2R_M}, \quad (5)$$

where  $\gamma$  is the angle between the magnetic and rotation axes. In this work, we assume that the WD is an aligned rotator for simplicity, that is,  $\gamma = 0^\circ$ . Therefore, the accumulation efficiency  $\eta_{\text{He}}(\dot{M}, M_{\text{wd}})$  is replaced by  $\eta_{\text{He}}(\dot{M}/f_{\text{pc}}, M_{\text{wd}})$  in the case of polar cap accretion (Ablimit & Maeda 2019a). We incorporated the above prescriptions into MESA (version r10398) (Paxton et al. 2015) to follow the evolution of the WD + He star binaries.

### 2.3. Binary Evolution

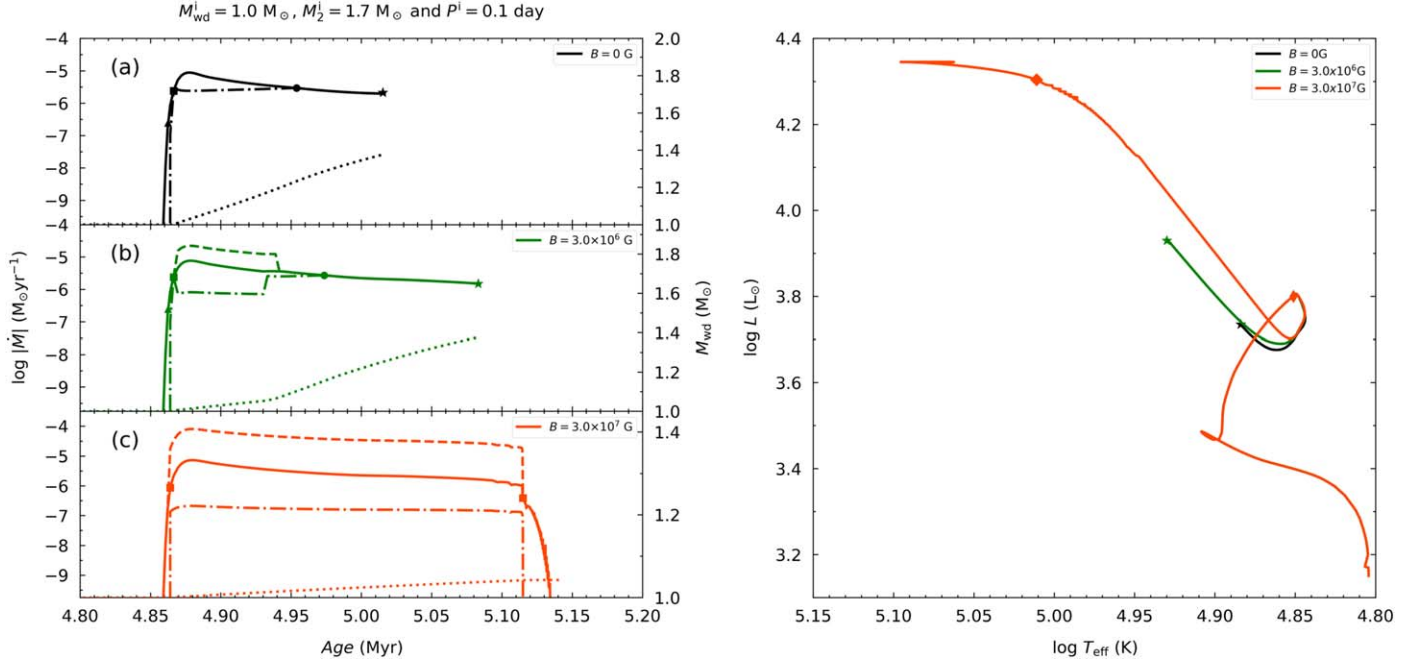
In order to demonstrate the influence of magnetic fields on the WD + He binary evolution, we construct several models with different surface magnetic field strengths  $B = 0, 3.0 \times 10^6$  and  $3.0 \times 10^7$  G. There are observational evidences indicating that the surface magnetic fields of the accretors (especially for neutron stars) decayed because of accretion (Taam & van den Heuvel 1986), caused by ohmic dissipation or screening of accreted matter (Geppert & Urpin 1994; Romani 1990). However, whether accretion can induce magnetic field decay in WDs is still debated, considering the fact that polars are strongly magnetized but old WDs have accreted for a very long time. For instance, AR UMa was classified as a polar in a binary system, but the magnetic field of the accreting WD is still as high as  $\sim 230$  MG (Ferrario et al. 2002). Thus, we do not take the magnetic field decay into consideration in our work due to its great uncertainties. In each model, the initial WD

masses  $M_{\text{wd}}^i$  are taken to be 0.858, 0.9, 0.95, 1.0, 1.05, 1.1, 1.15, 1.2 and  $1.25 M_{\odot}$  (the minimum initial mass for WDs that can evolve to SNe Ia is  $M_{\text{min}}^i = 0.858 M_{\odot}$  with the KH prescription, and  $M_{\text{min}}^i = 0.9 M_{\odot}$  with the WL prescription in the case of  $B = 0$  G), the initial He star masses  $M_2^i$  range from  $0.6 M_{\odot}$  to  $3.5 M_{\odot}$  by steps of  $0.05 M_{\odot}$ , and the initial orbital periods  $P^i$  (in units of days) vary logarithmically from  $-1.7$  to  $2.8$  by steps of  $0.1$ .

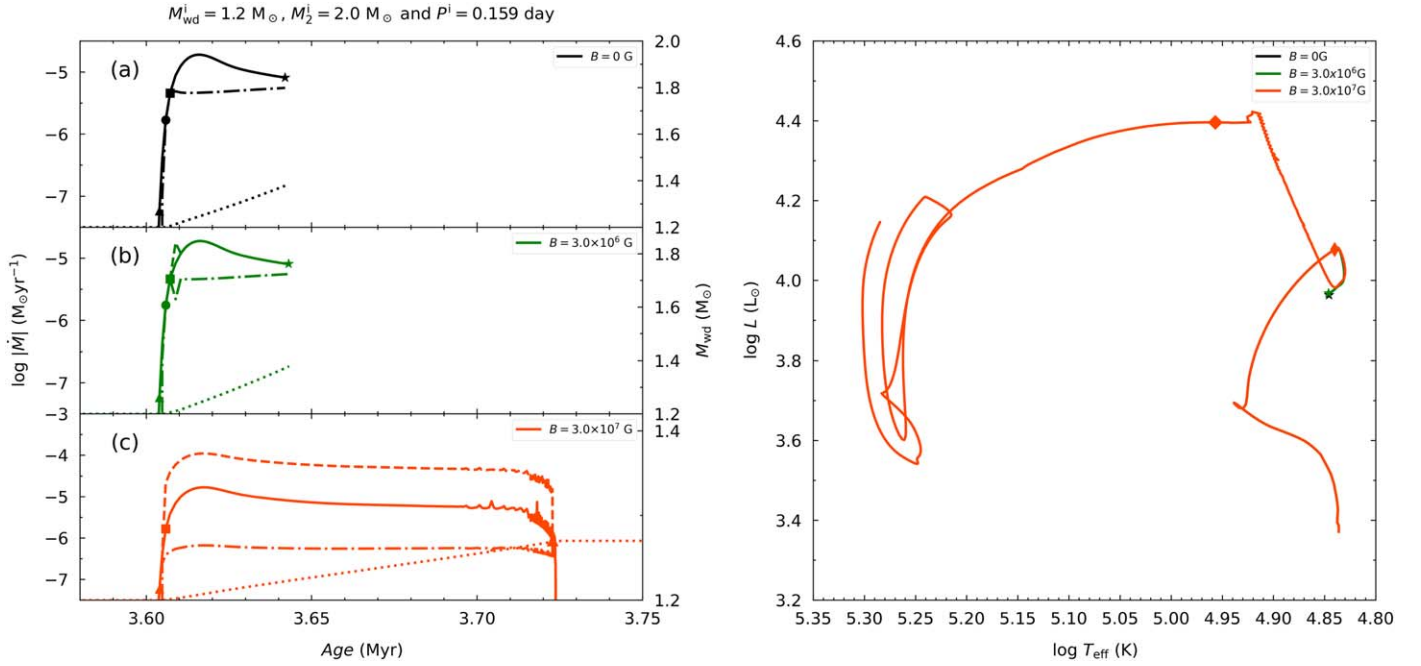
In the following, we display some representative examples with our binary evolution calculations.

Figure 1 shows the results of binary evolution with the initial parameters  $(M_{\text{wd}}^i/M_{\odot}, M_2^i/M_{\odot}, P^i/\text{day}) = (1.0, 1.7, 0.1)$ . Panels [a]-[c] in the left column depict the results of the non-magnetic ( $B = 0$  G), intermediate-magnetic ( $B = 3.0 \times 10^6$  G) and high-magnetic ( $B = 3.0 \times 10^7$  G) models, respectively. In the right column, we show the evolution of the companion stars in the Hertzsprung-Russell (H-R) diagram, and the moment when the WD is expected to explode in an SN Ia is labeled by an asterisk.

The mass transfer starts at the age of  $\sim 4.86$  Myr when the He donor expands and overflows its Roche lobe after the exhaustion of central helium. In the non-magnetic model (panel [a]), He-shell burning on the WD is initially unstable because  $\dot{M}$  is lower than the weak He-shell flash limit  $\dot{M}_{\text{low}}$ , so violent flashes prevent the mass growth of the WD. With the expansion of the He star's envelope and the contraction of the orbit,  $\dot{M}$  increases, the flashes weaken, and eventually the burning becomes thermally stable when  $\dot{M} \geq \dot{M}_{\text{stable}}$ . With further increase in  $\dot{M}$ , a radiation-driven wind is triggered at the age of 4.865 Myr, blowing away part of the accreted material. Steady nuclear burning is accordingly limited at a rate of  $\dot{M}_{\text{crit}} \simeq 3.2 \times 10^{-6} M_{\odot} \text{ yr}^{-1}$ . The wind phase ceases at the age of  $\sim 4.95$  Myr when  $\dot{M}$  drops below  $\dot{M}_{\text{crit}}$ . During this steady burning phase the binary can be identified as an SSS until the WD explodes in an SN. In the intermediate-magnetic model (panel [b]), the evolution process is the same as in the non-magnetic one until  $\sim 4.865$  Myr, when the magnetic confinement effect commences. Since the transformed rate  $\dot{M}/f_{\text{pc}}$  is higher than  $\dot{M}_{\text{crit}}$ , the mass accumulation is limited in the polar caps at a rate of  $f_{\text{pc}} \dot{M}_{\text{crit}}$ . After about 0.075 Myr, the magnetic confinement fails, and the WD evolves in a similar way as a non-magnetic WD. The WD explodes in the stable He-shell burning phase, 0.07 Myr later than in the non-magnetic model because of the lower mass growth rate of the WD. The binary parameters at the moment of the SN explosion are  $(M_{\text{WD}}^{\text{SN}}/M_{\odot}, M_2^{\text{SN}}/M_{\odot}, P^{\text{SN}}/\text{day}) = (1.378, 1.108, 0.09)$  in the non-magnetic model, and  $(1.378, 0.983, 0.098)$  in the intermediate-magnetic model. The surviving companion star in the intermediate-magnetic model is generally less massive and hotter than in the non-magnetic model, as depicted in the right column.



**Figure 1.** A representative case of binary evolution with  $M_{\text{wd}}^i = 1.0 M_{\odot}$ ,  $M_2^i = 1.7 M_{\odot}$  and  $P^i = 0.1$  day. The WL prescription is adopted for the He-rich mass accumulation efficiency. The left column shows the evolutionary history of the mass transfer rate  $\dot{M}$  (the solid lines), WD's mass accumulation rate  $\dot{M}_{\text{wd}}$  (the dashed-dotted lines),  $\dot{M}/f_{\text{pc}}$  (dashed lines in panel [b]–[c]) and the WD's mass  $M_{\text{wd}}$  (dotted lines) with different  $B$ -field strengths. The triangles, circles and squares mark  $|\dot{M}/f_{\text{pc}}| = \dot{M}_{\text{low}}$ ,  $\dot{M}_{\text{stable}}$  and  $\dot{M}_{\text{crit}}$ , respectively. The right panel displays the corresponding evolutionary tracks of the companion star in the HR diagram, with the thin diamond, thick diamond and asterisk symbols signifying the moments of contacting, detaching and SN explosions of systems respectively.



**Figure 2.** Same as Figure 1 but for systems with  $(M_{\text{wd}}^i, M_2^i, P^i) = (1.2, 2.0, 0.159)$ , and the KH prescription is used for the He-rich mass accumulation efficiency.

Evolution in the high-magnetic model (panel [c]) is quite different. As the magnetic confinement acts soon after the He-shell ignition until the end of the mass transfer, a substantial fraction of the He-rich matter is blown away from the WD by the super-Eddington wind, which stops at the age of  $\sim 5.12$  Myr. Then  $\dot{M}$  rapidly drops below  $\dot{M}_{\text{low}}$ , and strong He-shell flashes expel all the transferred matter. Because of the extensive mass loss, the WD can only grow up to  $1.05 M_{\odot}$ .

Figure 2 shows the binary evolution with the initial parameters  $(M_{\text{wd}}^i/M_{\odot}, M_2^i/M_{\odot}, P^i/\text{day}) = (1.2, 2.0, 0.159)$  in the non-magnetic [a] and magnetic ([b] and [c]) models with the KH prescription. Because the donor mass is more massive, the mass transfer rate is higher, and it is more difficult to confine the accreted matter. It can be seen that the evolution in the intermediate-magnetic model is almost the same as in the non-magnetic one, with the magnetic confinement working only for a very short time. The binary parameters at the moment of the SN explosion are  $(M_{\text{wd}}^{\text{SN}}/M_{\odot}, M_2^{\text{SN}}/M_{\odot}, P^{\text{SN}}/\text{day}) = (1.378, 1.556, 0.143)$  and  $(1.379, 1.546, 0.143)$  in the non- and intermediate-magnetic models, respectively. In the high-magnetic model, the magnetic confinement always works and  $\dot{M}/f_{\text{pc}}^*$  exceeds  $\dot{M}_{\text{crit}}$  soon after the onset of RLOF and until the mass transfer terminates, so the WD accumulates its mass at a rate of  $f_{\text{pc}}^* \dot{M}_{\text{crit}}$ . Because of the strong wind loss, the WD's mass fails to grow up to  $1.378 M_{\odot}$ .

Figure 3 summarizes the results of the WD + He star evolution for  $M_{\text{wd}}^i = 1.2 M_{\odot}$  with different magnetic field strengths and  $\eta_{\text{He}}$  prescriptions (KH: panels [a-c]; WL: panels [d-f]). Systems with the initial parameters located within the red curves are regarded as potential SN Ia progenitors. The filled triangles, circles and squares signify the WD binaries experiencing weak helium-shell flashes, steady helium-shell burning and optically thick wind at the moment of the SN explosion, respectively, and the crosses indicate systems in which the WDs fail to explode. We find that the results in the non- and intermediate-magnetic models are almost the same because the  $B$ -fields in the latter are generally lower than the minimum value of the magnetic field that can confine the matter. In the high-magnetic model, the magnetic confinement takes effects, and the parameter space for the SN progenitors shrinks toward shorter  $P^i$  and smaller  $M_2^i$ . The reason is that the magnetic confinement is more likely to trigger radiation-driven wind in systems with higher donor masses or longer periods, thus hampering efficient mass accumulation of the WDs in these binaries.

Figure 4 shows the initial distributions of the SN Ia progenitors on the  $P^i - M_2^i$  plane with different  $B$ -fields. The four panels correspond to  $M_{\text{wd}}^i = 1.0, 1.1, 1.15$  and  $1.2 M_{\odot}$  (the minimum  $M_{\text{wd}}^i$  that can form an SN Ia is  $0.858, 0.95$  and  $1.0 M_{\odot}$  in the non-, intermediate- and high-magnetic models,

respectively), respectively. It is obvious that the parameter spaces shrink toward shorter orbital periods and smaller donor masses with increasing  $B$ , and for a given magnetic field strength, the parameter spaces become larger for more massive  $M_{\text{wd}}^i$ . We also feature the corresponding results with the WL prescription in Figure 5. Since the stable He-burning region obtained by Wang et al. (2015) is substantially narrower than that by Nomoto (1982), the initial parameter space for the progenitors of SNe Ia with the WL prescription is considerably smaller than with the KH prescription. Only WDs more massive than  $1.2 M_{\odot}$  can evolve to SNe Ia if their magnetic fields are as high as  $3 \times 10^7$  G. These mean that the magnetic fields of WDs do not help stabilize helium burning on WDs, in contrast with the results for the hydrogen burning processes. To investigate their influence on the overall SN Ia production in our Galaxy, we perform BPS of the evolution of magnetized WDs and present the results in the next section.

### 3. Binary Population Synthesis of WD + He Binary Evolution

We use the BPS code originally developed by Hurley et al. (2002) to simulate the evolution of  $2 \times 10^7$  binaries until the formation of WD + He star binaries. Theoretically, the WD + He star binaries can form in three major ways (Wang & Han 2012),

1. MS + MS  $\rightarrow$  subgiant/FGB + MS  $\xrightarrow{\text{stable RLOF}}$  He star  
 + MS  $\xrightarrow{\text{stable RLOF}}$  CO WD + MS  $\xrightarrow{\text{dynamical unstable RLOF}}$   
 CE phase CE ejection  $\rightarrow$  CO WD + He star,
2. MS + MS  $\rightarrow$  EAGB star + MS  $\xrightarrow{\text{dynamical unstable RLOF}}$   
 CE phase  $\xrightarrow{\text{CE ejection}}$  He RG + MS  $\xrightarrow{\text{stable RLOF}}$  CO WD +  
 MS  $\xrightarrow{\text{dynamical unstable RLOF}}$  CE phase  $\xrightarrow{\text{CE ejection}}$  CO WD +  
 He star,
3. MS + MS  $\rightarrow$  TPAGB stage + He-core burning stage  
 $\xrightarrow{\text{dynamical unstable RLOF}}$  CE phase  $\xrightarrow{\text{CE ejection}}$  CO WD +  
 He star.

Here FGB, EAGB and TPAGB are the abbreviations of the stellar evolutionary stage of first giant branch, early asymptotic giant branch and thermally pulsating asymptotic giant branch, respectively. We then combine the properties of the WD + He star binaries from our BPS calculations with the subsequent evolutionary results calculated with the MESA code. If the parameters of the formed CO WD + He star systems are located in the parameter space featured in Figure 4 or Figure 5, we assume that it will explode as an SN Ia. From the calculated results we can obtain the birthrates and delay times of the SNe Ia, and the characteristics of the surviving companion stars.

In the BPS study, the initial primary star mass  $M_1$ , secondary star mass  $M_2$  and orbital separations  $a$  are set to be

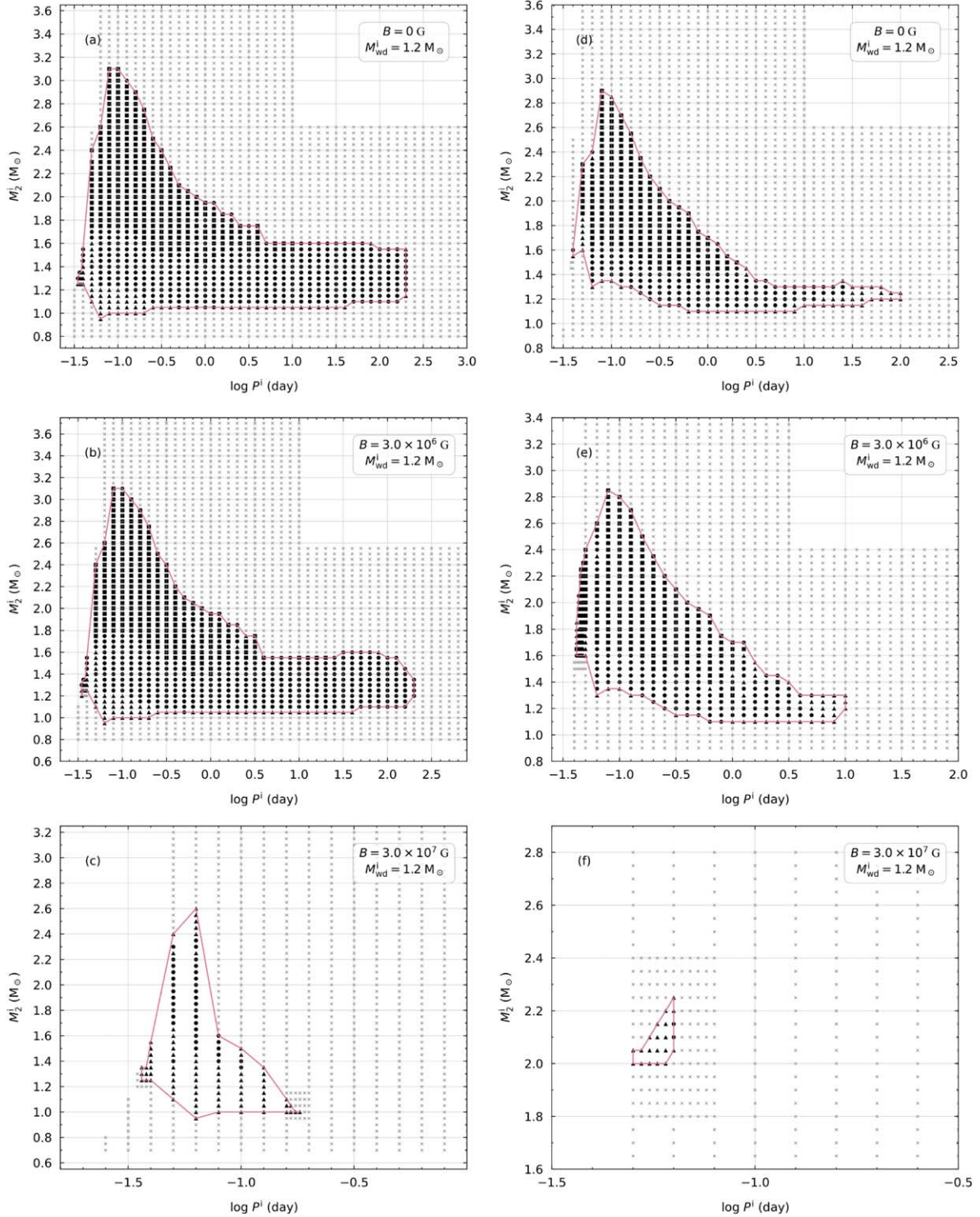


**Figure 3.** Distributions of the initial orbital period  $P^i$  and initial donor star mass  $M_2^i$  for the SN progenitor systems in the WD + He star channel with  $M_{\text{wd}}^i = 1.2 M_\odot$ . The KH prescription is adopted for the He-rich mass accumulation efficiency in panels [a]-[c] and the WL prescription in panels [d]-[f]. The three panels in each column correspond to  $B = 0$ ,  $3.0 \times 10^6$  and  $3.0 \times 10^7$  G, respectively. The triangles, circles and squares signify that the WDs in these systems are experiencing weak He-shell flashes, steady He-shell burning and optically thick wind (KH prescription) or super-Eddington wind (WL prescription) at the moment of the SN explosion, respectively. The crosses indicate systems that fail to explode owing to strong nova outbursts or wind mass loss from the WDs.

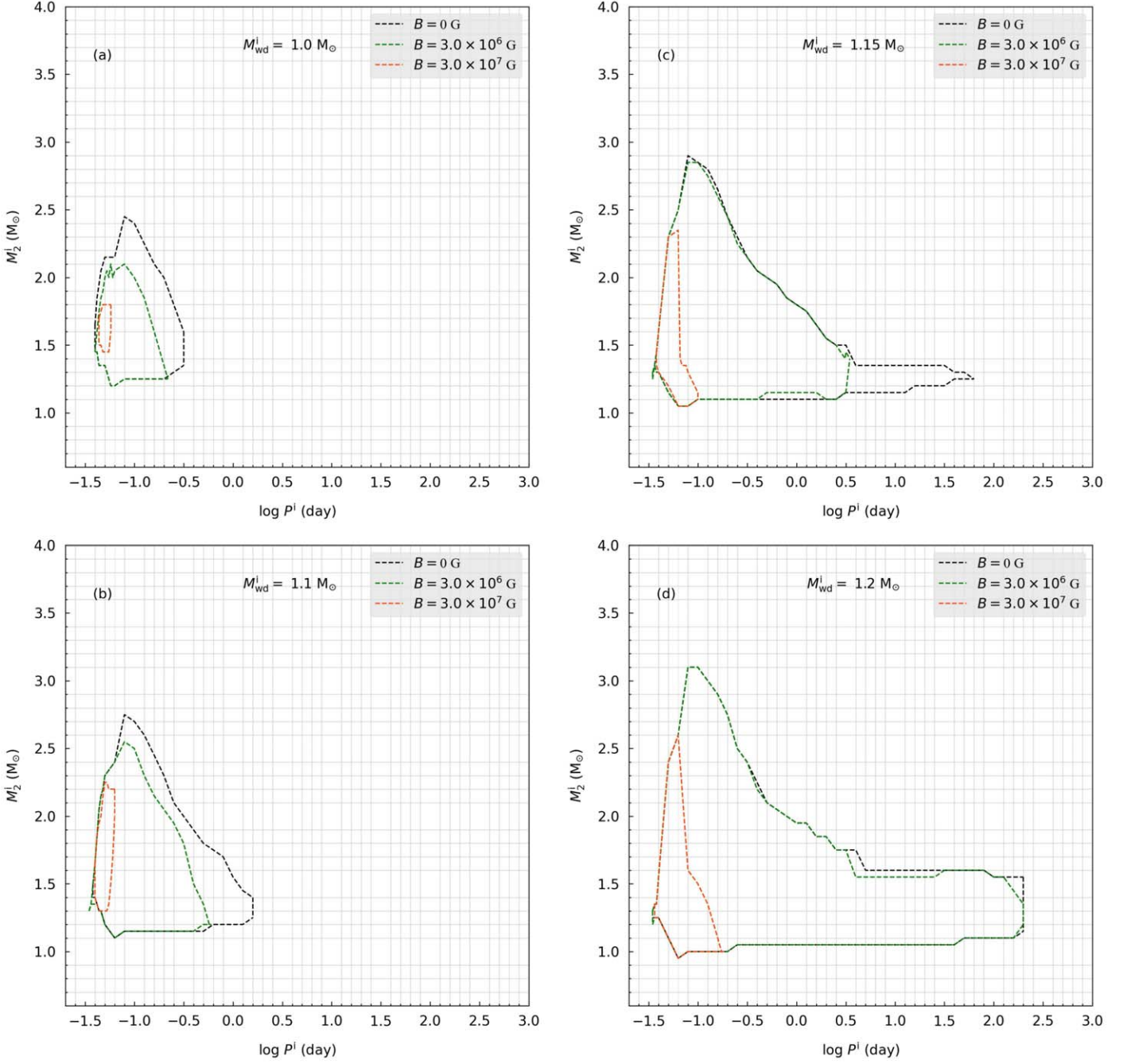


**Figure 4.** Distribution of the initial orbital period  $P^i$  and companion mass  $M_2^i$  for potential SN Ia progenitor systems with different  $M_{\text{wd}}^i$  and  $B$ -fields. The KH prescription is adopted for the He-rich mass accumulation efficiency. The four panels correspond to  $M_{\text{wd}}^i = 1.0M_{\odot}$  (panel [a]),  $1.1 M_{\odot}$  (panel [b]),  $1.15 M_{\odot}$  (panel [c]) and  $1.2 M_{\odot}$  (panel [d]), respectively. The black, green and orange-red curves represent the results with  $B = 0$ ,  $3.0 \times 10^6$  and  $3.0 \times 10^7$  G, respectively.

$0.8\text{--}40 M_{\odot}$ ,  $0.8\text{--}40 M_{\odot}$  and  $3\text{--}10^4 R_{\odot}$ , respectively. We assume that the distribution of  $M_1$  follows the initial mass function of Kroupa et al. (1993), the mass ratio  $q_2 = M_2/M_1$  is uniformly distributed within  $[0, 1]$  and the distribution of  $\ln a$  is also uniformly distributed. Same as Hurley et al. (2002), we assume one binary system with  $M_1 \geq 0.8 M_{\odot}$  is born in the

Galaxy per year, i.e., the star formation rate is  $7.6085 \text{ yr}^{-1}$ . When the mass transfer is dynamically unstable, a common envelope (CE) phase ensues, and the accreting star spirals into the donor's envelope. To deal with the CE evolution, we adopt the values of the binding energy parameter  $\lambda$  provided by Xu & Li (2010) for the envelope of the donor, and the

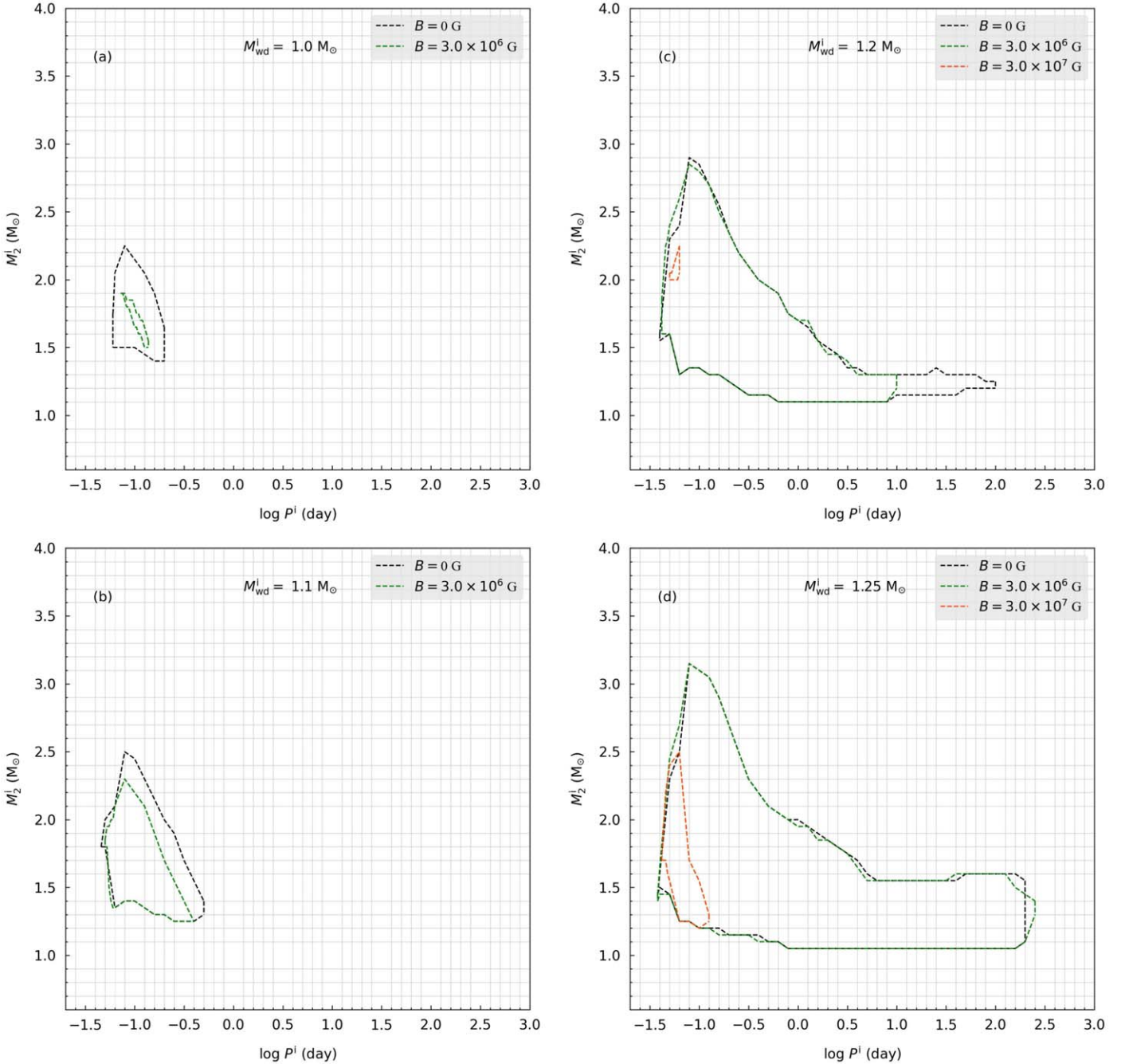


**Figure 5.** Same as Figure 4 but with the WL prescription adopted for the He-rich mass accumulation efficiency. Panels [a]–[d] correspond to  $M_{\text{wd}}^i = 1.0, 1.1, 1.2$  and  $1.25 M_{\odot}$ , respectively. Note that the minimal initial mass of a WD that can form an SN Ia is  $1.2 M_{\odot}$  in the high-magnetic model.

efficiency factor  $\alpha = 0.5$  and  $1.0$ . All the binaries are assumed to be in circular orbits.

Figures 6 and 7 display the companion star’s absolute magnitude in V-band ( $M_V$ ) and effective temperature ( $T_{\text{eff}}$ ) at the moment of the SN explosion, with  $\alpha = 0.5$  and  $1.0$  respectively. Here the He-rich mass accumulation efficiencies

are calculated with the KH prescription. Each panel demonstrates the results with a specific magnetic field strength, and the colors correspond to the magnitude of the SN birthrate. Next to each panel we show the histogram distribution of  $M_V$ . Both the non- and intermediate-magnetic models demonstrate similar bimodal distributions (the bright peak is provided by the

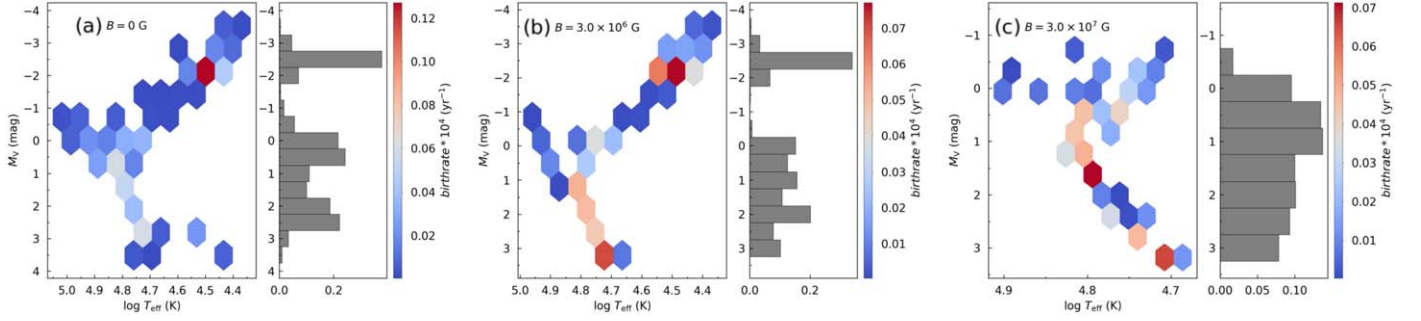


**Figure 6.** Distribution of the effective temperature and the absolute magnitude of the surviving companion at the moment of SN explosion with  $\alpha = 0.5$ . Panels from left to right feature the outcomes of  $B = 0$ ,  $3.0 \times 10^6$  and  $3.0 \times 10^7$  G, respectively. The horizontal histogram close to the right of each panel gives the birthrate distribution of  $M_V$ . The KH prescription is adopted for the He-rich mass accumulation efficiency. The colors of the hexagons indicate the birthrates of these systems.

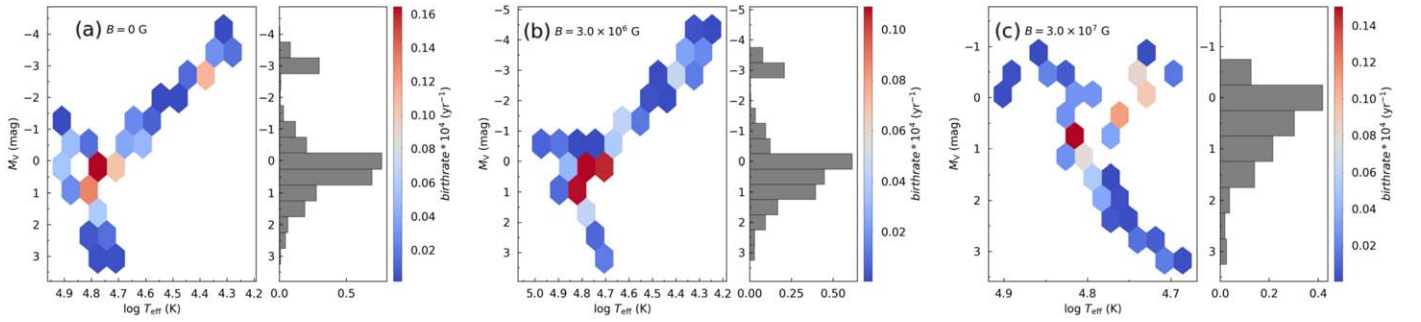


**Figure 7.** Same as Figure 6 but with  $\alpha = 1.0$ .

more massive donors in wide systems and the dim peak connotes the less massive ones in compact systems), while the distribution in the high-magnetic model is considerably narrower than in the former two models. A large fraction of the surviving companion stars are brighter than  $\sim -2.5^m$  when  $B = 0$  and  $3.0 \times 10^6$  G, but mainly dimmer than  $\sim 0^m$  when  $B = 3.0 \times 10^7$  G. Figure 7 also shows a bimodal  $M_V$  distribution, peaking at  $M_V \sim -3^m$  and  $0^m$  in both the non- and intermediate-magnetic models, while the  $M_V$  distribution is clustered around  $\sim 0^m$  in the high-magnetic model. Roughly speaking, the stronger the magnetic fields, the dimmer the surviving companions. One apparent difference between the results with  $\alpha = 0.5$  and  $\alpha = 1.0$  is that there are more surviving companions with  $M_V \sim 0^m - 1^m$  in the latter. They are the survivors of compact progenitor systems composed of a less massive He star, which are more likely merge during the CE phase with  $\alpha = 0.5$ . The brightness limits of the SN 2011fe’s progenitor system make it impossible for the companion to have mass  $\geq 3.5 M_\odot$  and  $M_V \leq 1^m$ , and rule out almost all the bright companions predicted from the RG-donor and He-donor channels (Li et al. 2011). However, quite a part of the companions in our high-magnetic models reveal  $M_V \geq 0^m$ , which are still compatible with the observations of SN 2011fe.

Our calculations also indicate that the surviving companions are characterized by relatively higher rotational velocities in the high-magnetic model than in the non- and intermediate-magnetic models. Figures 8 and 9 display the the rotational velocity  $v_{\text{rot}}$  versus the effective temperature  $T_{\text{eff}}$  of the companion star with  $\alpha = 0.5$  and 1.0, respectively. In the non- and intermediate-magnetic models generally  $v_{\text{rot}} \lesssim 150 \text{ km s}^{-1}$  and a large fraction of the surviving companions have  $v_{\text{rot}} \lesssim 10 \text{ km s}^{-1}$ . In the high-magnetic model the surviving companions possess a rotational velocity  $v_{\text{rot}} \sim 10\text{--}170 \text{ km s}^{-1}$ , which means that the binaries at the moment of SNe are relatively compact. This can be naturally explained by the initially narrow orbits of the progenitor binaries in the high-magnetic model.

Figures 10–13 display the distributions of the surviving companions calculated with the WL prescription. Figures 10 and 11 show the distribution in the  $M_V - T_{\text{eff}}$  plane, and Figures 12 and 13 in the  $v_{\text{rot}} - T_{\text{eff}}$  plane. We take  $\alpha = 0.5$  in Figures 10 and 12, and  $\alpha = 1.0$  in Figures 11 and 13. Generally speaking, Figures 10–13 follow the similar tendency as in Figures 6–9 with the KH prescription, but the birthrates are substantially lower than in the latter cases. In addition, the surviving companion stars are respectively slightly brighter and

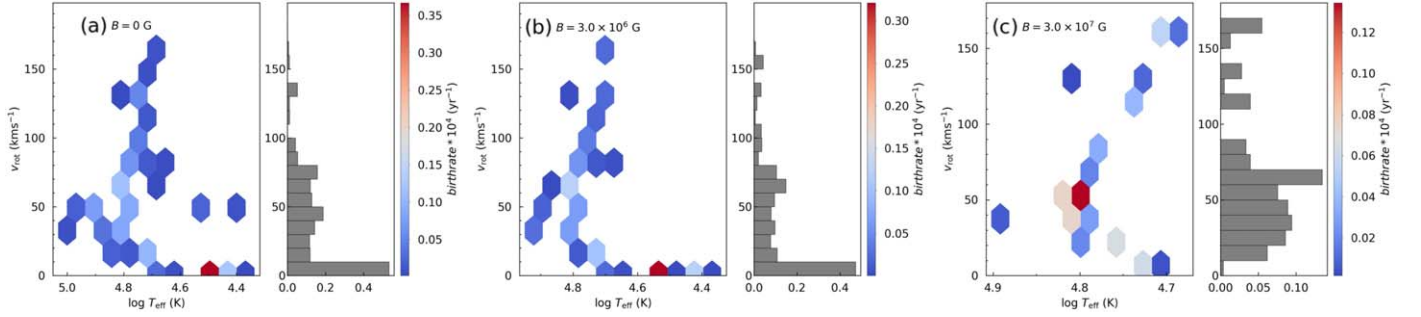


**Figure 8.** Distribution of the surface rotational velocity and effective temperature of the surviving companions at the moment of SN explosion with  $\alpha = 0.5$ . Panels from left to right display the outcomes with  $B = 0$ ,  $3.0 \times 10^6$  and  $3.0 \times 10^7$  G, respectively. Birthrate distribution of  $v_{\text{rot}}$  is also shown in the corresponding horizontal histogram. The colors of the hexagons indicate the corresponding birthrates of these systems.

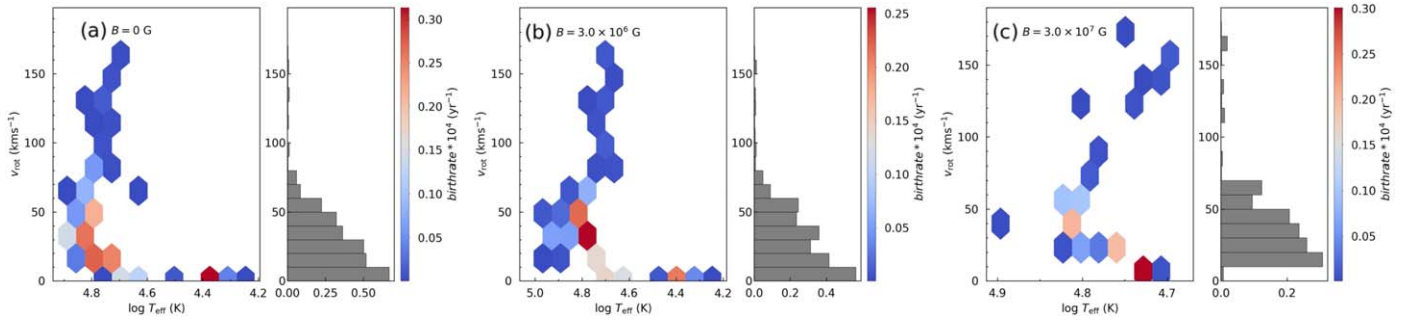


**Figure 9.** Same as Figure 8 but with  $\alpha = 1.0$ .

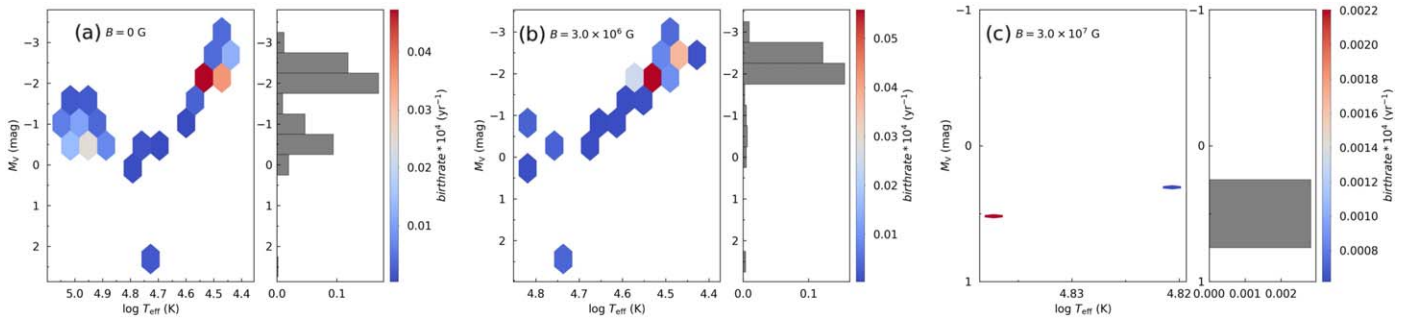


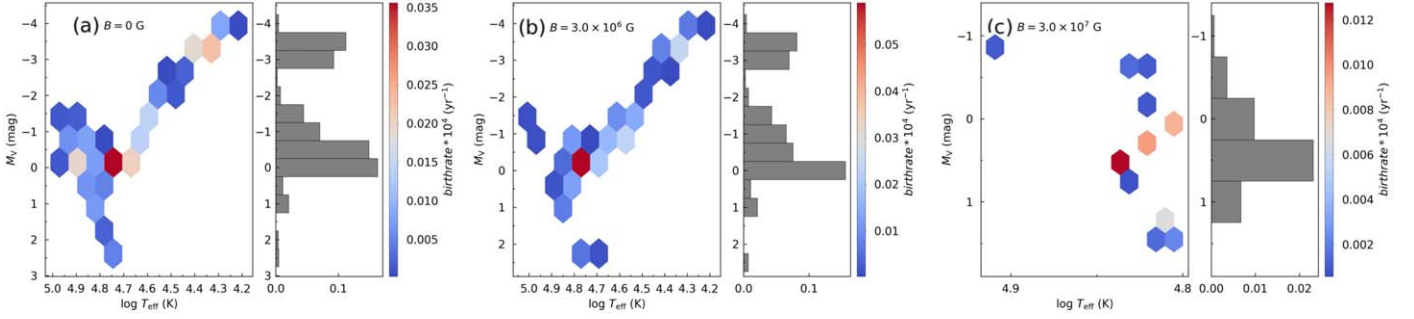
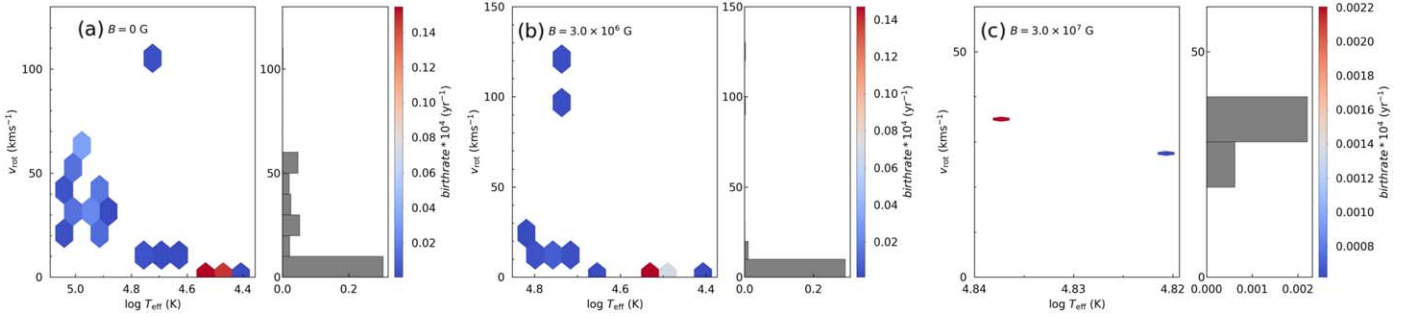
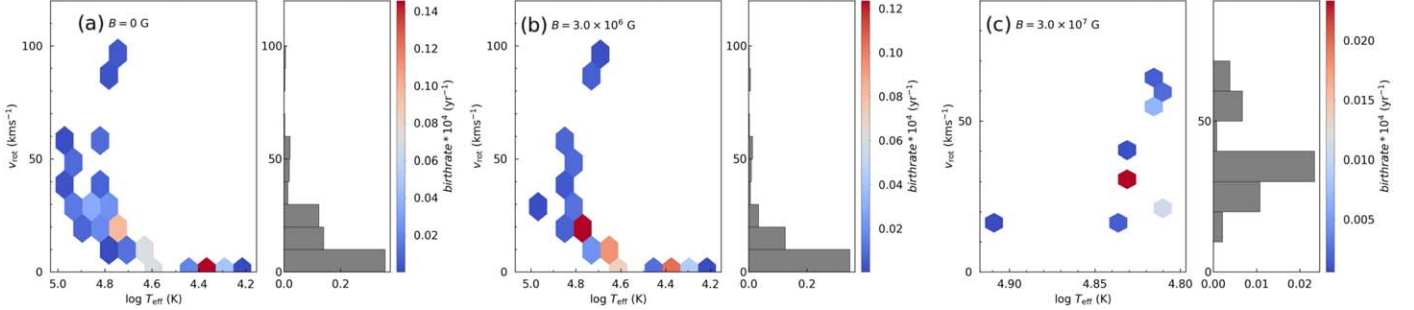
**Figure 10.** Same as Figure 6 but with  $\alpha = 0.5$  and the WL prescription for  $\eta_{\text{Hc}}$ .

dimmer in the non-/intermediate-magnetic and high-magnetic models compared with those in Figures 6–9.

Figures 14 and 15 show the DTD (left panel) and the cumulative birthrate evolution of SNe Ia (right panel) with the KH and WL prescriptions, respectively. The colors of the lines indicate different magnetic field strengths, and the results with  $\alpha = 0.5$  and 1.0 are displayed with dashed and solid lines, respectively. The DTD of SN Ia is defined as the time interval from the star formation to the SN explosion, which is dependent on the lifetimes of the progenitor binaries. The WD + He star channel links to relatively young populations.

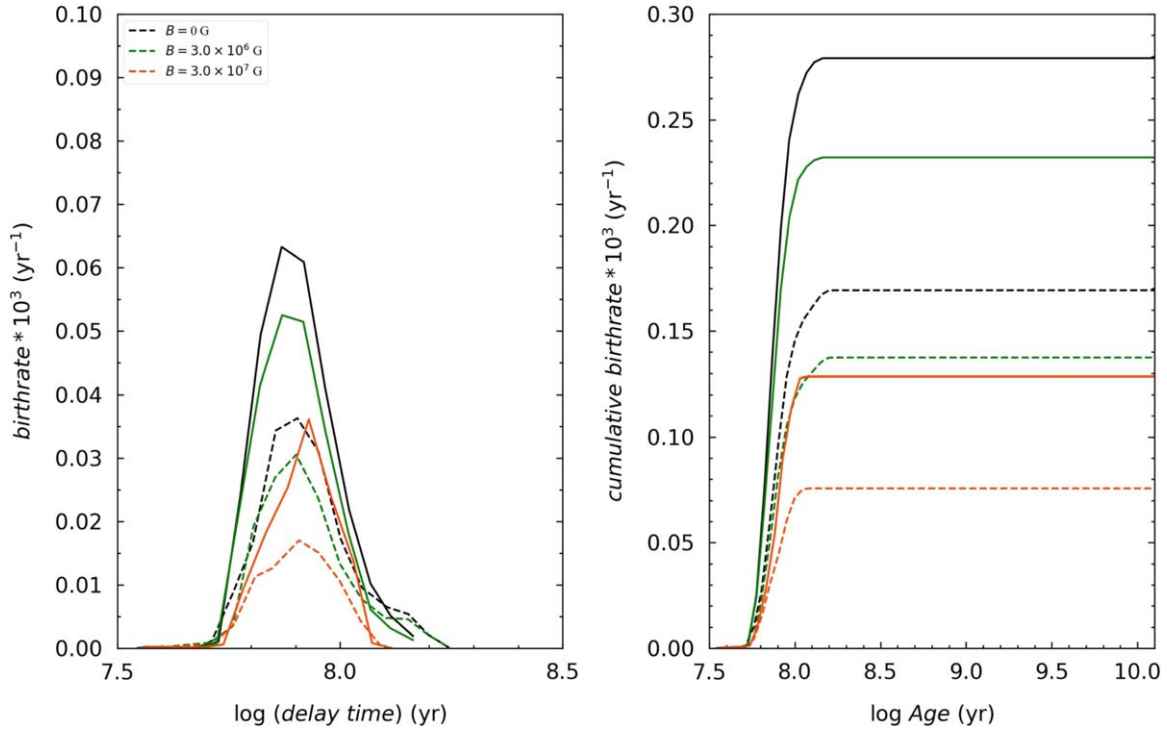
Figures 14 and 15 affirm that the delay times are  $\sim 35$ –160 Myr (KH) and  $\sim 35$ –126 Myr (WL) in both the non- and intermediate-magnetic models, and  $\sim 35$ –126 Myr (KH) and  $\sim 35$ –71 Myr (WL) in the high-magnetic models, respectively. The relatively short delay times in the high-magnetic models are due to the lack of the progenitor systems with wider initial orbits compared with those in the non- and intermediate-magnetic models, as depicted in Figures 3–5.

In Figure 14, the predicted birthrates of SNe Ia are  $\sim 0.17 \times 10^{-3} \text{ yr}^{-1}$  (with  $\alpha = 0.5$ ) and  $\sim 0.28 \times 10^{-3} \text{ yr}^{-1}$  (with  $\alpha = 1.0$ ) in the non-magnetic models,  $\sim 0.14 \times 10^{-3} \text{ yr}^{-1}$

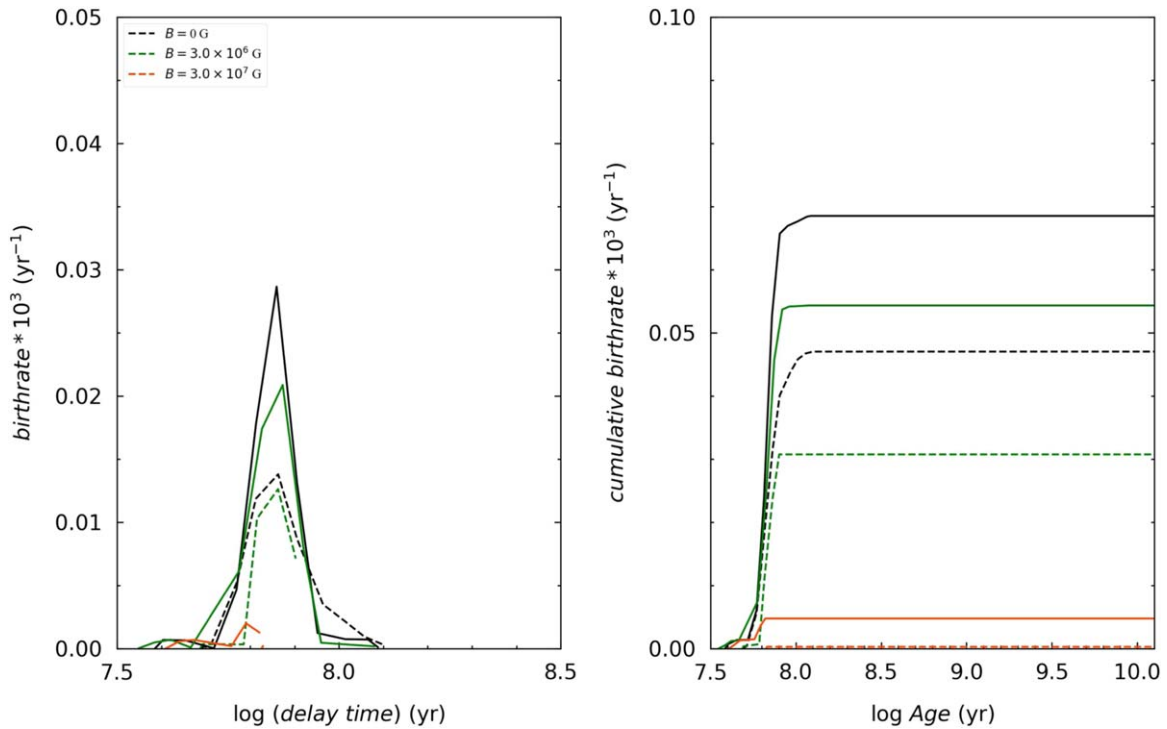

 Figure 11. Same as Figure 10 but with  $\alpha = 1.0$ .

 Figure 12. Same as Figure 8 but with the WL prescription for  $\eta_{\text{He}}$ .

 Figure 13. Same as Figure 12 but with  $\alpha = 1.0$ .

(with  $\alpha = 0.5$ ) and  $\sim 0.23 \times 10^{-3} \text{ yr}^{-1}$  (with  $\alpha = 1.0$ ) in the intermediate-magnetic model, and  $\sim 0.08 \times 10^{-3} \text{ yr}^{-1}$  (with  $\alpha = 0.5$ ) and  $\sim 0.13 \times 10^{-3} \text{ yr}^{-1}$  (with  $\alpha = 1.0$ ) in the high-magnetic models. The higher the  $B$ -fields are, the smaller the parameter space of the SN progenitors, and the lower the SN birthrates. In Figure 15, the birthrates with the WL prescription are significantly lower than in the corresponding models with the KH prescription, with the highest birthrate being  $\sim 0.07 \times 10^{-3} \text{ yr}^{-1}$  in the non-magnetic model with  $\alpha = 1.0$ . We also see in Figures 14 and 15 that the birthrates predicted with  $\alpha = 1.0$  are higher than those with  $\alpha = 0.5$  because the primordial binaries are more likely to survive the CE evolution with higher  $\alpha$ .

The predicted Galactic SN Ia birthrate in the high-magnetic models is  $\sim (0.08\text{--}0.13) \times 10^{-3} \text{ yr}^{-1}$  if all of the WDs are strongly magnetized, compared with  $\sim (0.17\text{--}0.28) \times 10^{-3} \text{ yr}^{-1}$  in the non-magnetic models. Considering the fact that about 25% of the WDs in binaries may be magnetic (Ferrario et al. 2015; Pala et al. 2020), the overall predicted birthrate is at most  $\sim (0.15\text{--}0.24) \times 10^{-3} \text{ yr}^{-1}$ . This is significantly lower than the Galactic SN Ia birthrate ( $\sim 5 \times 10^{-3} \text{ yr}^{-1}$ , e.g., Patat & Hallakoun 2018). However, the magnetic WD + He star channel is still worth investigating since the surviving companion stars predicted in this channel can be quite dim, providing a natural explanation for non-detection of bright surviving companions associated with some SNe Ia.



**Figure 14.** The left and right panels display the DTD distributions and the cumulative birthrates of SNe Ia, respectively. Here we adopt the KH prescription for  $\eta_{\text{He}}$ . The black, green and orange-red curves represent the results of non-magnetic, intermediate-magnetic and high-magnetic models, respectively. The dashed and solid lines correspond to the results of  $\alpha = 0.5$  and  $1.0$ , respectively.



**Figure 15.** Same as Figure 14 but with the WL prescription for  $\eta_{\text{He}}$ .

#### 4. Summary

In this paper, we investigate the contributions of the WD + He star binaries to SNe Ia by considering the WDs with non-, intermediate- and high-magnetic fields. With detailed binary evolution and BPS calculations we obtain the parameter space of potential SN Ia progenitors and the properties of the surviving companions. Compared with the case of non-magnetic accreting WDs, magnetically confined mass accretion makes it less possible for the WDs to steadily accumulate mass owing to mass loss from strong wind, meaning that the influence of the magnetic confinement on He-accreting WDs is quite different from that on H-accreting WDs. This is because the helium-ignition pressure  $P_b$  is typically  $\sim 10$ – $1000$  times higher than that for hydrogen-ignition, and increases with decreasing mass transfer rates. Thus it is difficult for the magnetic confinement to take effect and enhance the He-rich mass accumulation efficiency  $\eta_{\text{He}}$  in systems with relatively low  $\dot{M}$ . Our calculations demonstrate that the magnetic confinement does lead to different characteristics of the surviving companion stars, such as the mass, luminosity and rotational velocity distributions. However, the predicted overall birthrates are still significantly lower than the Galactic SN Ia birthrate. This further strengthens the notion that WD + He binaries, even with the effect of magnetic fields of the WDs taken into account, are not likely to be the primary progenitors of SNe Ia.

#### Acknowledgments

We are grateful to an anonymous referee for a careful reading of the manuscript and helpful comments. This work was supported by the Natural Science Foundation of China (Grant Nos. 11773015, 12121003, 12041301) and Project U1838201 supported by NSFC and CAS.

#### ORCID iDs

Zhe Cui  <https://orcid.org/0000-0001-8311-0608>

#### References

- Ablimit, I., & Maeda, K. 2019a, *ApJ*, **871**, 31  
 Ablimit, I., & Maeda, K. 2019b, *ApJ*, **885**, 99  
 Ablimit, I., Xu, X.-J., & Li, X. D. 2014, *ApJ*, **780**, 80  
 Alam, U., Sahni, V., & Starobinsky, A. A. 2007, *JCAP*, **2007**, 011  
 Badenes, C., Hughes, J. P., Bravo, E., & Langer, N. 2007, *ApJ*, **662**, 472  
 Branch, D., Romanishin, W., & Baron, E. 1996, *ApJ*, **465**, 73  
 Branch, D., & Tammann, G. A. 1992, *ARA&A*, **30**, 359  
 Brooks, J., Bildsten, L., Schwab, J., & Paxton, B. 2016, *ApJ*, **821**, 28  
 Brown, P. J., Dawson, K. S., de Pasquale, M., et al. 2012, *ApJ*, **753**, 22  
 Cappellaro, E., & Turatto, M. 1997, in NATO Advanced Study Institute (ASI) Ser. C, 486, *Thermonuclear Supernovae*, ed. P. Ruiz-Lapuente, R. Canal, & J. Isern (Kluwer Academic), 77  
 Cappellaro, E., Turatto, M., Tsvetkov, D. Y., et al. 1997, *A&A*, **322**, 431  
 Demianski, M., Piedipalumbo, E., Sawant, D., & Amati, L. 2019, arXiv:1911.08228  
 Dimitriadis, G., Rojas-Bravo, C., Kilpatrick, C. D., et al. 2019, *ApJL*, **870**, L14  
 Ferrario, L., de Martino, D., & Gänsicke, B. T. 2015, *SSRv*, **191**, 111  
 Ferrario, L., Wickramasinghe, D., & Kawka, A. 2020, *AdSpR*, **66**, 1025  
 Ferrario, L., Wickramasinghe, D. T., & Schmidt, G. 2002, in ASP Conf. Ser. 261, *The Physics of Cataclysmic Variables and Related Objects*, ed. B. T. Gänsicke, K. Beuermann, & K. Reinsch (San Francisco, CA: ASP), 149  
 Frank, J., King, A., & Raine, D. J. 2002, *Accretion Power in Astrophysics* (3rd edn; Cambridge: Cambridge University Press)  
 Gänsicke, B. T., Euchner, F., & Jordan, S. 2002, *A&A*, **394**, 957  
 Geppert, U., & Urpin, V. 1994, *MNRAS*, **271**, 490  
 Hachisu, I., Kato, M., & Nomoto, K. 1996, *ApJL*, **470**, L97  
 Hameury, J. M., King, A. R., & Lasota, J. P. 1986, *MNRAS*, **218**, 695  
 Hamuy, M., Maza, J., Phillips, M. M., et al. 1993, *AJ*, **106**, 2392  
 Hamuy, M., Phillips, M. M., Maza, J., et al. 1991, *AJ*, **102**, 208  
 Hamuy, M., Phillips, M. M., Suntzeff, N. B., et al. 1996, *AJ*, **112**, 2391  
 Han, Z., & Podsiadlowski, P. 2004, *MNRAS*, **350**, 1301  
 Hirsch, H. A., Heber, U., O'Toole, S. J., & Bresolin, F. 2005, *A&A*, **444**, L61  
 Hoefflich, P., & Khokhlov, A. 1996, *ApJ*, **457**, 500  
 Hurley, J. R., Tout, C. A., & Pols, O. R. 2002, *MNRAS*, **329**, 897  
 Iben, I. J., & Tutukov, A. V. 1984, *ApJS*, **54**, 335  
 Iwamoto, K., Brachwitz, F., Nomoto, K., et al. 1999, *ApJS*, **125**, 439  
 Kato, M., & Hachisu, I. 2004, *ApJL*, **613**, L129  
 Kato, M., Hachisu, I., Kiyota, S., & Saio, H. 2008, *ApJ*, **684**, 1366  
 Kelly, P. L., Fox, O. D., Filippenko, A. V., et al. 2014, *ApJ*, **790**, 3  
 Kepler, S. O., Pelisoli, I., Koester, D., et al. 2015, *MNRAS*, **446**, 4078  
 Kerzendorf, W. E., Schmidt, B. P., Asplund, M., et al. 2009, *ApJ*, **701**, 1665  
 Kerzendorf, W. E., Strampelli, G., Shen, K. J., et al. 2018, *MNRAS*, **479**, 192  
 Kerzendorf, W. E., Yong, D., Schmidt, B. P., et al. 2013, *ApJ*, **774**, 99  
 Kroupa, P., Tout, C. A., & Gilmore, G. 1993, *MNRAS*, **262**, 545  
 Külebi, B., Jordan, S., Euchner, F., Gänsicke, B. T., & Hirsch, H. 2009, *A&A*, **506**, 1341  
 Leonard, D. C. 2007, *ApJ*, **670**, 1275  
 Li, W., Bloom, J. S., Podsiadlowski, P., et al. 2011, *Natur*, **480**, 348  
 Li, X. D., & van den Heuvel, E. P. J. 1997, *A&A*, **322**, L9  
 Liu, D., Wang, B., & Han, Z. 2018, *MNRAS*, **473**, 5352  
 Liu, D. D., Wang, B., Podsiadlowski, P., & Han, Z. 2016, *MNRAS*, **461**, 3653  
 Livio, M. 1983, *A&A*, **121**, L7  
 Lü, G., Zhu, C., Wang, Z., & Wang, N. 2009, *MNRAS*, **396**, 1086  
 Lundqvist, P., Nyholm, A., Taddia, F., et al. 2015, *A&A*, **577**, A39  
 Maeda, K., & Terada, Y. 2016, *IJMPD*, **25**, 1630024  
 Mannucci, F., Della Valle, M., Panagia, N., et al. 2005, *A&A*, **433**, 807  
 Maoz, D., & Mannucci, F. 2008, *MNRAS*, **388**, 421  
 Maoz, D., & Mannucci, F. 2012, *PASA*, **29**, 447  
 Maoz, D., Mannucci, F., Li, W., et al. 2011, *MNRAS*, **412**, 1508  
 Maoz, D., Mannucci, F., & Nelemans, G. 2014, *ARA&A*, **52**, 107  
 Maoz, D., Sharon, K., & Gal-Yam, A. 2010, *ApJ*, **722**, 1879  
 Mazzali, P. A., Röpke, F. K., Benetti, S., & Hillebrandt, W. 2007, *Science*, **315**, 825  
 Neunteufel, P., Yoon, S. C., & Langer, N. 2017, *A&A*, **602**, A55  
 Nomoto, K. 1982, *ApJ*, **253**, 798  
 Nomoto, K., & Iben, I. J. 1985, *ApJ*, **297**, 531  
 Nomoto, K., Iwamoto, K., & Kishimoto, N. 1997, *Sci*, **276**, 1378  
 Nugent, P., Baron, E., Branch, D., Fisher, A., & Hauschildt, P. H. 1997, *ApJ*, **485**, 812  
 Olling, R. P., Mushotzky, R., Shaya, E. J., et al. 2015, *Natur*, **521**, 332  
 Osborne, J. P., Borozdin, K. N., Trudolyubov, S. P., et al. 2001, *A&A*, **378**, 800  
 Pala, A. F., Gänsicke, B. T., Breedt, E., et al. 2020, *MNRAS*, **494**, 3799  
 Patat, F., & Hallakoun, N. 2018, arXiv:1805.03207  
 Paxton, B., Marchant, P., Schwab, J., et al. 2015, *ApJS*, **220**, 15  
 Perlmutter, S., Aldering, G., Goldhaber, G., et al. 1999, *ApJ*, **517**, 565  
 Phillips, M. M. 1993, *ApJL*, **413**, L105  
 Piersanti, L., Tornambé, A., Yungelson, L., & Straniero, O. 2013, in *Binary Paths to Type Ia Supernovae Explosions*, ed. R. Di Stefano, M. Orto, & M. Moe, Vol. 281 (Dordrecht: Kluwer Academic), 209  
 Piersanti, L., Tornambé, A., & Yungelson, L. R. 2014, *MNRAS*, **445**, 3239  
 Rest, A., Scolnic, D., Foley, R. J., et al. 2014, *ApJ*, **795**, 44  
 Riess, A. G., Filippenko, A. V., Challis, P., et al. 1998, *AJ*, **116**, 1009  
 Riess, A. G., Strolger, L.-G., Casertano, S., et al. 2007, *ApJ*, **659**, 98  
 Romani, R. W. 1990, *Natur*, **347**, 741  
 Ruiter, A. J., Belczynski, K., & Fryer, C. 2009, *ApJ*, **699**, 2026  
 Ruiz-Lapuente, P. 2014, *NewAR*, **62**, 15  
 Ruiz-Lapuente, P., Damiani, F., Bedin, L., et al. 2018, *ApJ*, **862**, 124

- Sand, D. J., Graham, M. L., Botyánszki, J., et al. 2018, *ApJ*, 863, 24
- Schaefer, B. E., & Collazzi, A. C. 2010, *AJ*, 139, 1831
- Schaefer, B. E., & Pagnotta, A. 2012, *Natur*, 481, 164
- Schmidt, G. D., Harris, H. C., Liebert, J., et al. 2003, *ApJ*, 595, 1101
- Shappee, B. J., Stanek, K. Z., Pogge, R. W., & Garnavich, P. M. 2013, *ApJL*, 762, L5
- Shen, K. J., & Bildsten, L. 2009, *ApJ*, 699, 1365
- Shen, K. J., Bildsten, L., Kasen, D., & Quataert, E. 2012, *ApJ*, 748, 35
- Sion, E. M., Holberg, J. B., Oswald, T. D., et al. 2014, *AJ*, 147, 129
- Soker, N., & Gilkis, A. 2017, *ApJ*, 851, 95
- Taam, R. E., & van den Heuvel, E. P. J. 1986, *ApJ*, 305, 235
- Tucker, M. A., Shappee, B. J., & Wisniewski, J. P. 2019, *ApJL*, 872, L22
- Umeda, H., Nomoto, K., Yamaoka, H., & Wanajo, S. 1999, *ApJ*, 513, 861
- Vanlandingham, K. M., Schmidt, G. D., Eisenstein, D. J., et al. 2005, *AJ*, 130, 734
- Wang, B., & Han, Z. 2009, *A&A*, 508, L27
- Wang, B., & Han, Z. 2012, *NewAR*, 56, 122
- Wang, B., & Han, Z.-W. 2010, *RAA*, 10, 681
- Wang, B., Li, X.-D., & Han, Z.-W. 2010, *MNRAS*, 401, 2729
- Wang, B., Li, Y., Ma, X., et al. 2015, *A&A*, 584, A37
- Wang, B., Meng, X., Chen, X., & Han, Z. 2009, *MNRAS*, 395, 847
- Wang, B., Podsiadlowski, P., & Han, Z. 2017, *MNRAS*, 472, 1593
- Wheeler, J. C. 2012, *ApJ*, 758, 123
- Wheeler, J. C., Iben, & Iben, J. 1973, *ApJ*, 186, 1007
- Wickramasinghe, D. T., & Ferrario, L. 2000, *PASP*, 112, 873
- Woosley, S. E., Taam, R. E., & Weaver, T. A. 1986, *ApJ*, 301, 601
- Wu, C., Wang, B., Liu, D., & Han, Z. 2017, *A&A*, 604, A31
- Xu, X.-J., & Li, X.-D. 2010, *ApJ*, 722, 1985
- York, D. G., Adelman, J., Anderson, J. E. J., et al. 2000, *AJ*, 120, 1579
- Yungelson, L. R., & Kuranov, A. G. 2017, *MNRAS*, 464, 1607